Silicon
https://doi.org/10.1007/s12633-024-02947-4

RESEARCH

Synthesis and Optical Properties of Erbium-Doped Sodium Silicate in Sol-Gel Matrix

A. M. Mansour[1] · Ali B. Abou Hammad[1] · Amany M. El Nahrawy[1]

Received: 11 November 2023 / Accepted: 8 March 2024

Abstract
In this study, we investigated how the concentration of erbium (0.0, 1, 2 mol% Er) affects the structural and optical properties of thin films made from sol-gel sodium silicate doped with erbium nitrate, thermally treated at 250 °C. Through systematic investigation, we explore the structural evolution and optical behavior of the thin films across varying Er^{3+} concentrations. The sol-gel demonstrated effective capabilities for substantial concentrations of Er^{3+} oxides through doping at lower calcination temperatures. The spectroscopic characteristics were studied using visible-near infrared spectroscopy (UV–vis–NIR), transmission electron microscopy, and Fourier transform infrared spectroscopy. Increasing the Er ratio decreased both the transmission and the energy band gap (3.6–3.34 eV) of the films while the absorption peak increased. The obtained results suggest that Er^{3+} activators demonstrate advantageous optical properties in the evaluated sodium silicate glass matrix. With the introduction of Er, optical transmittance ranges from 85 to 55% in the visible and near-infrared (NIR) regions, highlighting their advantageous characteristics. This research contributes to advancing the understanding of erbium-doped thin films for potential applications in optoelectronic devices and photonics.

Keywords Erbium · Optical properties · Band gap energy · Silicate · Sol Gel · XRD

1 Introduction

Erbium garners significant attention as a commonly studied rare earth ion when integrated into an insulating matrix. The spectroscopic properties of Er ions and the optical features of sodium silicate nanoparticles have been extensively explored within a diverse range of host matrices, including sol-gel glasses [1–3]. Erbium ions hold substantial importance across various scientific and technological domains due to their unique properties and applications. Erbium-doped fiber amplifiers (EDFAs) are vital components in optical communication networks [4–6]. When pumped with light, erbium ions can efficiently amplify optical signals without frequent electronic regeneration. This enables long-distance and high-capacity data transmission [7, 8]. Erbium-doped fibers are employed in the development of sensitive fiber optic sensors. Changes in the surrounding environment, such as temperature or strain, can alter the fluorescence characteristics of the erbium ions, allowing for precise measurements.

Erbium-based materials are investigated for their role in improving solar cell efficiency and enhancing light absorption in photovoltaic devices [9, 10]. As stated by Hench and Vasconcelos [11], the sol-gel technique covers the concurrent hydrolysis and polycondensation of an alkoxide, like $Si(OR)_4$, where R can be CH_3, C_2H_5OH, or C_3H_7 [2, 11, 12]. The arrangement of the resulting condensed materials is influenced by factors such as pH, concentration of alkoxide, choice of solvents, presence and quantity of additives and dopants, gelation temperature, drying, and duration [13–17]. A variety of glass compositions, spanning fluorides, silicates, borates, and phosphates, have found application as matrix materials for accommodating trivalent rare-earth ions in the creation of dynamic optical tools. These tools encompass lasers, converters that shift light from infrared to visible wavelengths, phosphorescent materials, and more. Of these, silicate glasses stand out as a particularly well-researched subset.

The sol-gel method offers a versatile and scalable approach for crafting diverse systems such as perovskite, ceramics, and thin films. Recent developments in sol-gel

✉ Ali B. Abou Hammad
abohmad2@yahoo.com

[1] Solid State Physics Department, Physics Research Institute, National Research Centre (NRC), 33 El-Bohouth St., Dokki, Cairo 12622, Egypt

Published online: 22 March 2024

techniques have shown promise in producing ultrafine oxide glasses and ceramic composites [18–20]. This method provides advantages such as high purity, lower sintering temperatures, homogeneity, quick processing, and environmental friendliness [21–23]. With precise control over film thickness and composition, sol-gel facilitates the making of innovative materials, exemplified by Er-doped sodium silicate thin films, featuring customized optical properties and contributing to advancements in various technological domains.

The study of sodium silicate@Er^{3+} holds significant importance from spectroscopic application. Erbium-doped semiconductors are crucial in the development of optoelectronic devices such as optical amplifiers, lasers, and fiber optic communications systems [24–26]. By understanding how erbium concentration affects the structural and optical properties of sodium silicate, researchers can optimize the performance of these devices for improved efficiency and reliability [26, 27]. Moreover, sodium silicate is a versatile material widely used in various industries including coatings, adhesives, and ceramics [20, 28].

The development of the amorphous sodium silicate phase, followed by crystallization, takes place when uniformly prepared sodium silicate sol-gel precursors are subjected to controlled temperatures exceeding 250 °C. Additionally, high-purity sol-gel derived silica-based materials typically exhibit nanoscale dimensions [21, 29, 30]. Because vibrational spectroscopy reacts to its local surroundings, the objective of this investigation is to scrutinize the optical and FTIR spectra of α-sodium silicate. The uniqueness of Er-doped sodium silicate thin films prepared using sol-gel at 200 °C lies in the unique combination of several key features. Firstly, the low preparation temperature of 200 °C represents an energy-efficient and cost-effective process, making it suitable for various applications, especially optical communication and sensing technologies [31, 32]. Moreover, the introduction of Erbium (Er) as a dopant brings forth auspicious optical attributes, potentially augmenting the performance of the film in optoelectronic devices [10, 32, 33]. Sol-gel erbium-doped sodium silicate is a composite material synthesized through the sol-gel process, where erbium ions are incorporated into a sodium silicate matrix. This process involves the hydrolysis and condensation of precursor molecules to form a gel, followed by drying and annealing to obtain the final product [34–36].

Erbium doping introduces erbium ions (Er^{3+}) into the sodium silicate matrix, imparting unique optical and structural properties to the material [37, 38]. These properties make sol-gel erbium-doped sodium silicate attractive for various applications in optoelectronics, photonics, and materials science.

This examination extends to the impact of Er ions, intending to gain comprehensive insights into structural features and spectroscopic properties. Additionally, the study aims to explore the behavior of refractive indices and analyze chemical alterations, specifically in the context of reversible rearrangements within the intermediate range order. This paper presents findings on the optical and spectroscopic characteristics of novel erbium-doped sodium silicate thin films, suggesting their suitability for future applications in optical technologies.

2 Experimental

The chemicals used in this study were sodium nitrate ($Na(NO_3)_2{\cdot}6H_2O$, Aldrich), tetraethylorthosilicate ($Si(OC_2H_5)_4$, TEOS; Fluka), erbium nitrate; absolute ethanol (EtOH, commercial-grade), and hydrochloric acid (HCl, commercial grade). The sodium silicate thin films containing Er^{3+} (0, 1, and 2 mol%) were synthesized through the sol-gel process. The procedure involved dissolving the required quantity of sodium nitrate ($Na(NO_3)_2{\cdot}6H_2O$) in a mixture of H_2O, absolute ethanol, and HCL to create a sodium solution. The molarity of the Er solution was adjusted based on the desired dopant concentration (0, 1, or 2 mol%). Simultaneously, in a separate container, an erbium nitrate solution was prepared by dissolving the appropriate amount of erbium nitrate in a mixture of H_2O, absolute ethanol, and HCL, with the concentration tailored to achieve the desired dopant concentration. Ensure that both solutions are thoroughly mixed and homogeneous. Tetraethyl-orthosilicate is added to absolute ethanol/HCl under stirring continuously, before mixing with Na and Na/Er solutions. The gel can now be used for film deposition using dip-coating onto glass substrates. Allow the films to dry at 35 ^{o}C, removing any residual solvent. Then, films calcined at 250 ^{o}C to further consolidate the film structure and densification.

2.1 Characterization

The prepared thin films will be characterized using techniques such as Fourier transform infrared spectra, X-ray diffraction (XRD), transmission electron microscopy (TEM), and UV-Vis-spectrophotometer to confirm their structure, composition, and properties.

The Fourier transform infrared spectra (FTIRs) for each film were recorded between 400 and 4000 cm^{-1} for 32 scans by a (Thermo Nicolet-380) spectrometer, with a resolution of (0.5 cm^{-1}). The particle of films was checked by (TEM) (JEM-2100, Jeol, Japan).

The optical properties were verified by (Jasco, V-570) optical spectrophotometer in the range of 0.2–2.5 µm.

3 Results and Discussion

3.1 FTIR

The FTIR spectra of the newly developed Erbium-Doped Sodium Silicate, as depicted in Fig. 1, reveal an evident hump at 3440 cm^{-1}, arising from the symmetric stretching and bending vibrational modes of OH^- ions and absorbed water molecules. An additional, weaker peak around 2900 cm^{-1} is associated with the hydrogen bonding of ethyl groups introduced as a solvent [39, 40]. The 1649 cm^{-1} peak likely arises from the asymmetric stretching of OH groups and the stretching and bending modes of absorbed water molecules [39]. Notably, an intense band at 1093 cm^{-1} is attributed to the asymmetric stretching of Si–O–Si bonds, while a strong peak at 798 cm^{-1} corresponds to the symmetric stretching of Si–O–Si bonds [41, 42]. Another medium peak at 459 cm^{-1} may be attributed to the bending modes of O–Si–O bonds [42, 43]. The vibrational modes of all functional groups in the samples undergo a relative change. However, when lower molar ratios of this component are present in the glasses, no significant changes in vibrational modes related to Er^{3+} are observed [43].

3.2 XRD Study

Figure 2 displays the X-ray diffraction (XRD) patterns of sodium silicate specimens doped with Er. The XRD pattern of the films reveals that they exhibit an almost amorphous character with a certain degree of crystallinity. The apex of the amorphous halo is observed at $2\theta = 19.2^{o}$ to 28.5^{o}. The amorphous peak tip in all the sol-gel films is slightly shifted towards lower angles. This shift in the peak position suggests the generation of microstrain on the surface due to the introduction of Er ions, as discussed in reference [44–46]. As observed, the sample containing (2 mol%) Er^{3+} demonstrates a crystalline phase at $2\theta = 22.10°$ and 25.3°, consistent with the reported sodium silicate literature (PDF4 00-029-1261), along with the presence of some amorphous phase (Fig. 2c). The broadening of the peak and the alteration in intensity can be attributed to the successful incorporation of Er into the sodium silicate structure.

3.3 TEM

TEM micrographs in Fig. 3 illustrate the morphological features of sodium silicate films subjected to modification with Er^{3+} at two different concentrations (0 and 2 mol% Er) and subsequent calcination at 250 °C. The films doped with Er^{3+} displayed a consistent and well-defined shape, characterized by the presence of nano-spherical nanoparticles (Fig. 3a, b). This phenomenon can be attributed to the heightened cross-linkage of Er within the sodium silicate matrix, facilitating efficient interpenetration throughout the sodium silicate-based precursor. This favorable interaction promotes the formation of -Si–O–Na-O- and Er-O-Si bonds, contributing to the formation of more spherical and aggregated larger particles during the aging phase of the sol-gel process. Well-connected nanoparticles (-Si–O–Na-O- and Er-O-Si) suggest a network-like arrangement. The clustering of particles had appeared sufficient dispersion during the sol-gel synthesizing process, as confirmed by the particle distribution (Fig. 3c), indicating controlled nucleation and

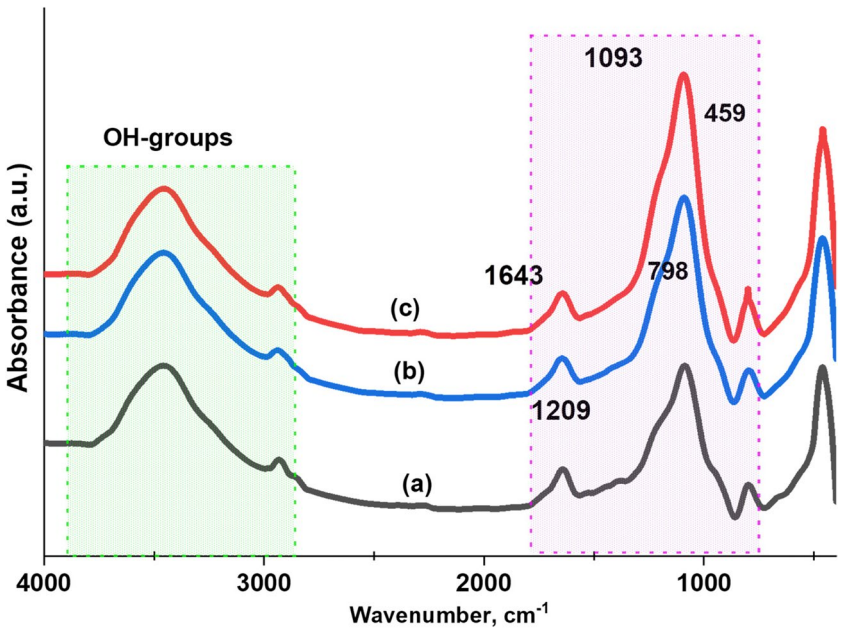

Fig. 1 FTIR spectra of (**a**) sodium silicate and sodium silicate system doped with (**b**) 1 (**c**) 2 Er^{3+}

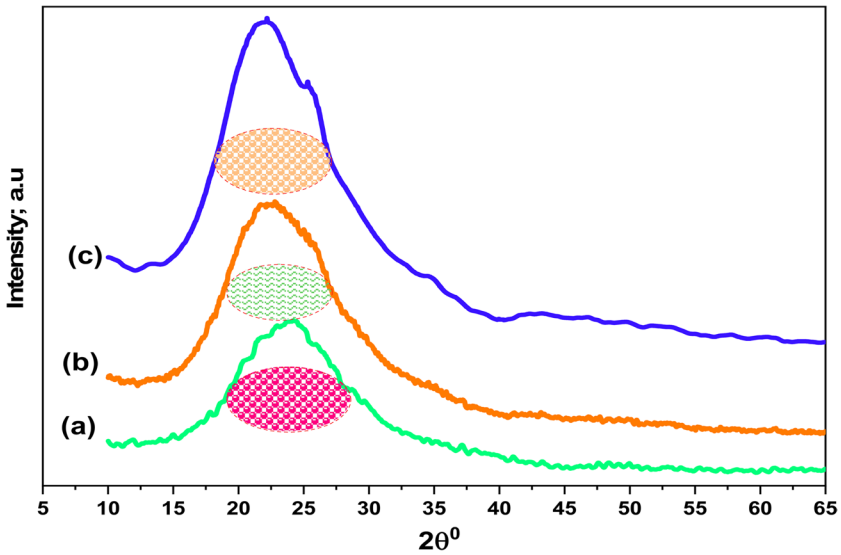

Fig. 2 XRD pattern of (**a**) sodium silicate and sodium silicate system doped with (**b**) 1 and (**c**) 2 Er^{3+}

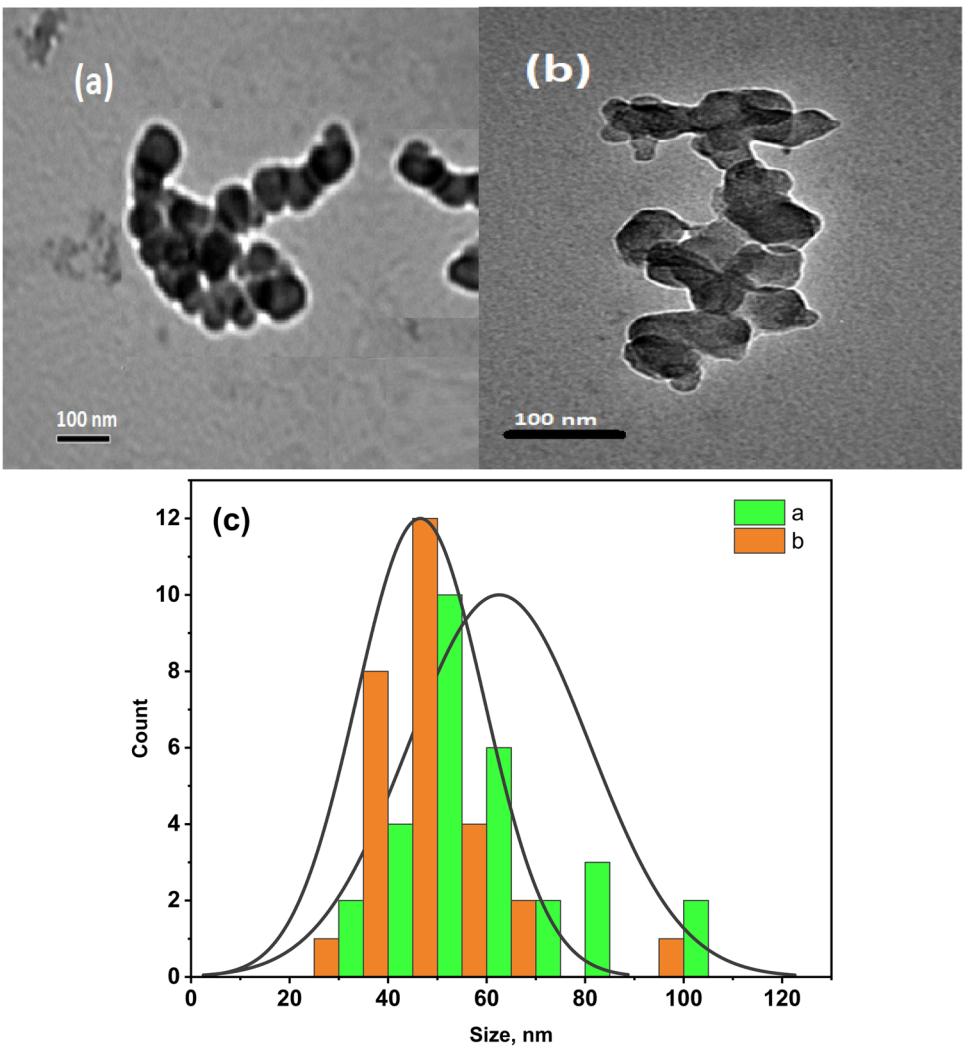

Fig. 3 TEM images of (**a**) sodium silicate and doped with (**b**) 2 Er^{3+}, and (**c**) particles distribution

growth. Figure 3c provides insights into the distribution of these particles in the Er/sodium silicate samples, indicating observable variations in the produced specimens. The average particle sizes in the films were found to range from 43 nm for the unmodified sodium silicate film to 51 nm for the Er-doped sodium silicate film.

3.4 Optical Studied

In semiconductors, the generation of charge carriers is initiated by optical photons. The absorption phenomenon in any material occurs due to several critical factors [47]: charge carrier electrons, valence band electrons, excitation of electrons, and inner shell electrons. In semiconductors, the valence band is occupied by electrons. During the absorption process, excitation occurs, leading these electrons to higher energy levels [48]. When photons with sufficient energy interact with semiconductor materials, they cause a quantized transfer of electrons from the valence band to the conduction band [49]. There are two significant types of optical transitions in semiconductor materials: direct transition and indirect transition. Both involve interactions with electrons in the valence band. However, direct band gap transitions are characterized by a direct vertical movement of electrons from the valence band to the conduction band [50]. In contrast, indirect band gap transitions involve simultaneous interactions with lattice vibrations or phonons [46]. In a direct band gap transition, the moment when electrons stabilize aligns with energy conservation principles. Conversely, in indirect band gap transitions, the moment when electrons move is influenced by phonon interactions [51].

UV-visible spectroscopy serves as a valuable tool for identifying the energy band gap values and types of materials by analyzing the transmitted radiation [52]. This analysis is based on the absorption of photons by electrons in their respective energy orbits. During this process, electrons transition from lower energy levels to higher energy levels and occur at specific energy levels known as the band gap energy [53]. This rise in energy levels during the absorption process is referred to as the absorption edge. At this absorption edge, the optical band gap energies can be precisely determined [36].

The optical transmittance and reflectance of the prepared samples were taken using the UV-Vis-NIR spectrophotometer with an integrating sphere using un-polarized light at room temperature. Figure 4 shows the optical transmittance and reflectance spectra of Erbium-Doped Sodium Silicate prepared by sol-gel with different Er-doping concentrations recorded in the wavelength range of 200 − 2500 nm. All samples showed good optical transmittance of 85% down to 55% with Er addition in the visible and near infra-red (NIR) region. The reflectance is very small (less than 10%) and it shows an increase with the increase of Er.

From the transmittance and reflectance, the absorption coefficient (α) is calculated and represented in Fig. 5. The optical absorption coefficient (α) was evaluated using the following relation using the optical transmittance (T) and thickness (t) values [17]:

$$\alpha = \ln(T/t)$$

From Fig. 5, it can be observed that the absorption coefficient increases with the addition of Er at all wavelengths

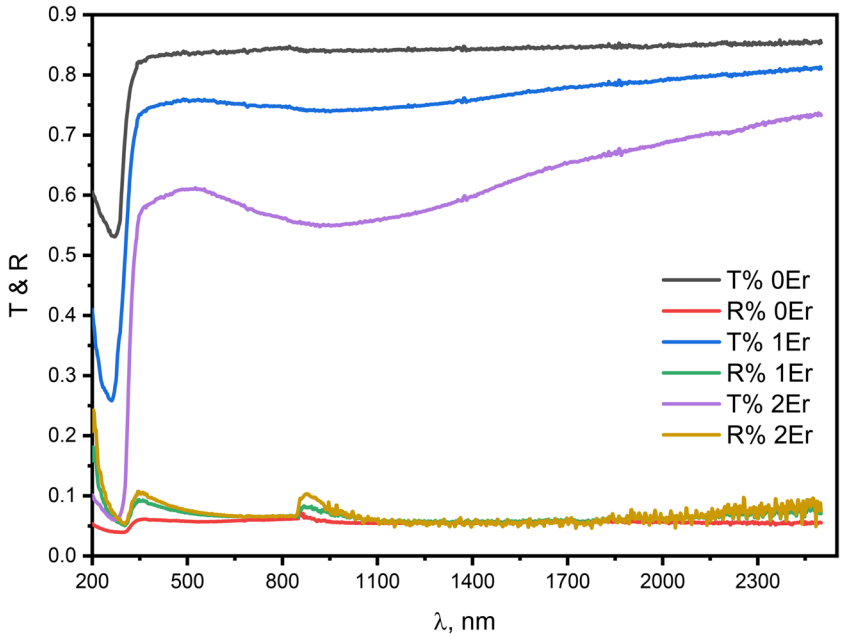

Fig. 4 The optical transmittance and reflectance spectra of Erbium-Doped Sodium Silicate prepared by sol-gel with different Er-doping concentrations recorded in the wavelength range of 200 − 2500 nm

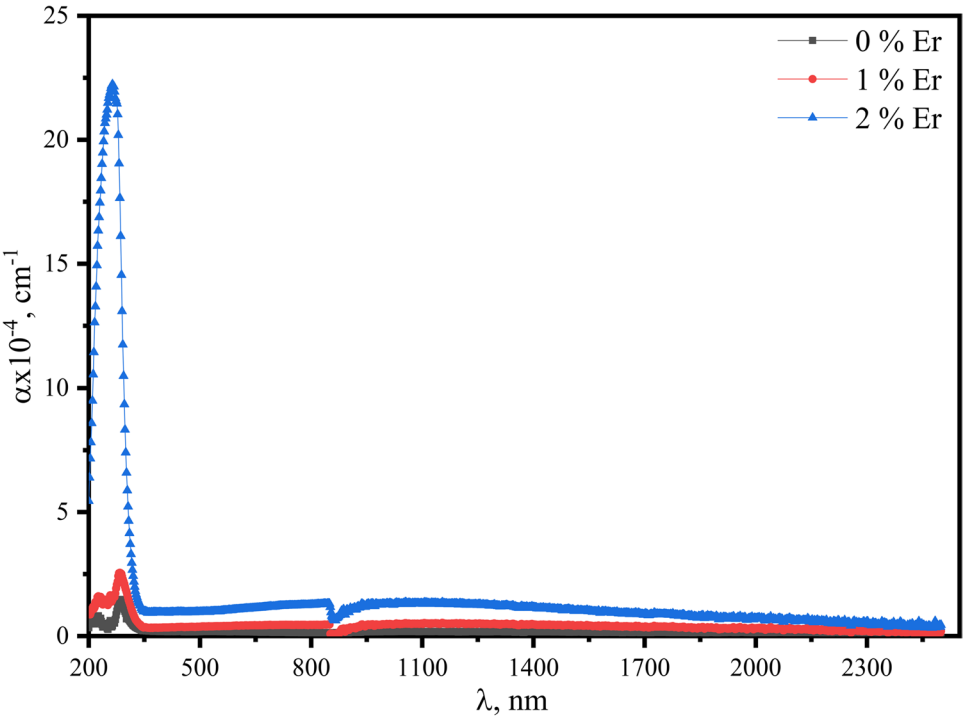

Fig. 5 The absorption coefficient of Erbium-Doped Sodium Silicate prepared by sol-gel with different Er-doping concentrations recorded in the wavelength range of 200 – 2500 nm

and there is a sharp absorption peak at about 270 nm for all samples. The intensity of the absorption peak increases slightly by the addition of 1 mol% Er and then increases sharply to high values by the addition of 2 mol% Er.

The band gap can be estimated from the absorption edge by using the Tauc relationship [54]. In this process, the change of absorption coefficient (α) in the strong absorption range is linked to the optical band gap (Eg) by the following relation [55],

$$\alpha h\upsilon = A(h\upsilon - E_g)^n$$

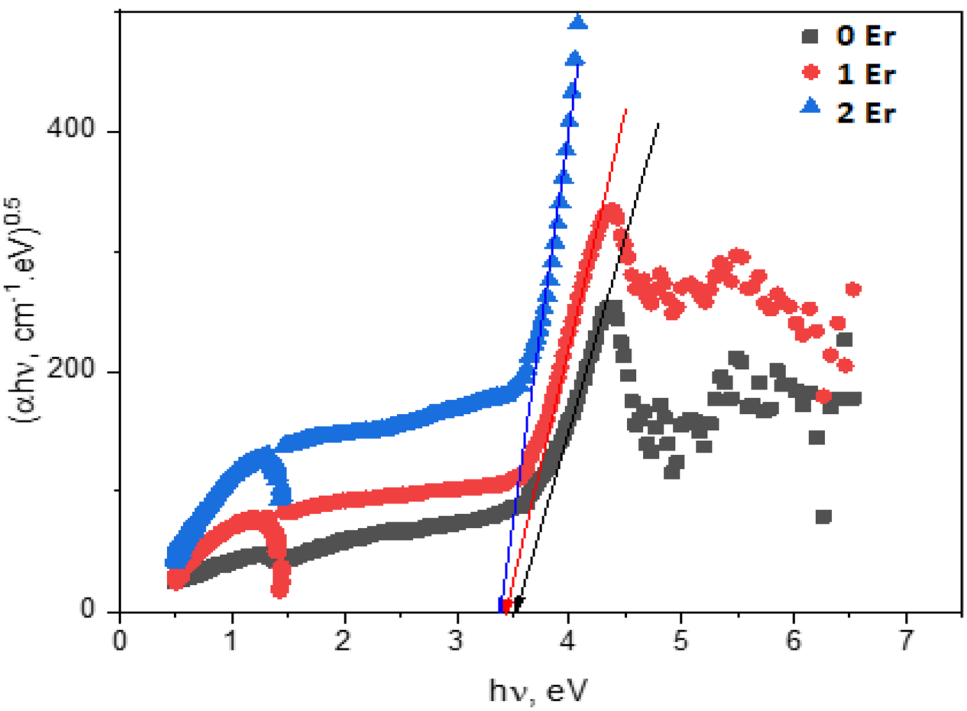

Fig. 6 The plot of $(\alpha h\nu)^{1/2}$ versus hυ

where

Eg band gap energy,

A an energy-independent constant,

n characteristic nature of the optical absorption type.

The electronic transition between the valance and conduction band can be direct or indirect. The value of n equals 2 and 3 for allowed and forbidden direct transitions respectively [16]. Also, the value of n equals 1/2 and 3/2 for allowed and forbidden indirect transitions respectively [56]. Since the transition in our case is direct, the index n equals 2.

The optical band gap of the samples was evaluated by extrapolation of the linear part of $(\alpha h\nu)^{1/2}$ versus hυ plot [57]. Figure 6 shows a similar plot for Erbium-Doped Sodium Silicate prepared in the present investigation. The evaluated energy band gap was 3.6–3.34 eV form pure to 2 Er samples. The amorphous nature of glass compositions typically results in an indirect band gap transition, whereas crystalline materials commonly exhibit a direct band gap transition. A reduction in the bandgap of sodium silicate, induced by Er doping, implies the integration of Er ions, potentially causing modifications in the electronic structure.

4 Conclusion

The study highlights the effectiveness of the sol-gel method in incorporating substantial amounts of Er^{3+} oxides into the sodium silicate matrix, even at lower calcination temperatures. This finding underscores the practicality and versatility of the sol-gel process for producing erbium-doped thin films, offering promising opportunities for applications in various industries.

The FTIR measurements suggested that the presence of Erbium oxide caused the breakdown of non-bridging Si-O bonds, converting them into bridging Si–O-Na and Si-O-Er bonds within the sodium silicate structure. X-ray diffraction (XRD) analysis confirmed the amorphous nature of the prepared films. The introduction of Er induced the disruption of Si–O–M bonds (where M represents Si, Na, and -OH) and resulted in the creation of Si–O–Er and Si–O–Na–O–Er bonds within the network structure. The film samples exhibited a noticeable tendency toward crystallization with increasing Er content, which was correlated with higher Er content, and significantly influenced both the structure and optical properties of the prepared films. These insights provide a deeper understanding of the structural modifications induced by Er^{3+} doping in sodium silicate at lower temperatures, which is valuable for various applications in materials science and nanotechnology. In addition, as the content of Er increased, there was a discernible decrease in the bandgap values for the nanofilms. This decline can be ascribed to the growing number of non-bridging oxygen (NBO) sites, as the addition of SiO_2 introduces greater disorder into the sodium silicate network. These insights provide a deeper understanding of the structural modifications induced by Er^{3+} doping in sodium silicate, which is valuable for various applications in optical nanotechnology.

Acknowledgements The work was not financially supported, and the National Research Centre of Egypt facilitates the work and the characterization tools.

Author Contributions Amany Mohamed El Nahrawy: conceived and designed the experiments; analyzed and interpreted the data; contributed reagents, materials, analysis tools, or data; wrote the paper. Ali B. Abou Hammad, A.M. Mansour: analyzed and interpreted the data; contributed reagents, materials, analysis tools, or data; wrote the paper.

Funding Open access funding provided by The Science, Technology & Innovation Funding Authority (STDF) in cooperation with The Egyptian Knowledge Bank (EKB).

Data Availability Not available.

Declarations

This research doesn't involve Human Participants and/or Animals.

Ethics Approval Not applicable.

Consent to Participate Authors confirm their participation.

Consent for Publication The authors confirm their acceptance for Publication.

Competing Interests The authors declare no competing interests.

References

1. Abou Hammad AB, Bakr AM, Abdel-Aziz MS, El Nahrawy AM (2020) Exploring the ferroelectric effect of nanocrystalline strontium zinc titanate/Cu: Raman and antimicrobial activity. J Mater Sci: Mater Electron 31:7850–7861. https://doi.org/10.1007/S10854-020-03323-9
2. Oréfice RL, Vasconcelos WL (1997) Sol-gel transition and structural evolution on multicomponent gels derived from the

alumina-silica system. J Sol-Gel Sci Technol 9(3):239–249. https://doi.org/10.1023/A:1018303226682
3. Elnahrawy AM, Kim YS, Ali AI (2016) Synthesis of hybrid chitosan/calcium aluminosilicate using a sol-gel method for optical applications. J Alloys Compd 676:432–439. https://doi.org/10.1016/J.JALLCOM.2016.03.210
4. Lu YW, Huang C, Cheng JG, Larsen AN (2016) High Er3 + luminescent efficiency in Er-doped SiOx films containing amorphous Si nanodots. J Alloys Compd 676:428–431. https://doi.org/10.1016/j.jallcom.2016.03.184
5. Tholkappiyan R, Vishista K (2015) Combustion synthesis of Mg-Er ferrite nanoparticles: Cation distribution and structural, optical, and magnetic properties. Mater Sci Semicond Process 40:631–642. https://doi.org/10.1016/j.mssp.2015.06.076
6. Yang S, Nie Y, Zhang B et al (2020) Construction of Er-doped ZnO/SiO2 composites with enhanced antimicrobial properties and analysis of antibacterial mechanism. Ceram Int 46:20932–20942. https://doi.org/10.1016/J.CERAMINT.2020.05.149
7. Haoran L, Chang-An W, Chenguang Z, Shuyan T (2015) Thermo-physical properties of rare-earth hexaaluminates LnMgAl11O19 (ln: La, Pr, Nd, Sm, Eu and Gd) magnetoplumbite for advanced thermal barrier coatings. J Eur Ceram Soc 35:1297–1306. https://doi.org/10.1016/j.jeurceramsoc.2014.10.030
8. Okasha N, El-Dek SI, Ayman M, Ali AI (2016) Comparative study on the influence of rare earth ions doping in Bi0.6Sr0.4FeO3nanomultiferroics. J Alloys Compd 689:1051–1058. https://doi.org/10.1016/j.jallcom.2016.08.077
9. Dahshan A, Hammad ABA, Aly KA, El Nahrawy AM (2020) Eu2O3 role in the optical and photoluminescence properties of 50SiO2-7MgO-20ZnO-(23-x)La2O3-xEu2O3 nano-crystalline thin films. Appl Phys A Mater Sci Process 126. https://doi.org/10.1007/S00339-019-3207-3
10. Battisha IK, Salem MA, Nahrawy AMS et al (2009) Erbium activated monolith silica-phosphate glasses planar waveguide and up-conversion mechanism. Int J Nano Biomater 2:191–203. https://doi.org/10.1504/IJNBM.2009.027713
11. Hench LL, Vasconcelos W (1990) Gel-silica science. Annu Rev Mater Sci 20:269–298. https://doi.org/10.1146/ANNUREV.MS.20.080190.001413
12. Li S, Zhang Y, Lin S et al (2021) Effects of nano-SiO2 coated multi-walled carbon nanotubes on mechanical properties of cement-based composites. Constr Build Mater 281:122577. https://doi.org/10.1016/J.CONBUILDMAT.2021.122577
13. Kumar RV, Anupama AV, Kumar R et al (2018) Cation distributions and magnetism of Al-substituted CoFe2O4 - NiFe2O4 solid solutions synthesized by sol-gel auto-combustion method. Ceram Int 44:20708–20715. https://doi.org/10.1016/j.ceramint.2018.08.065
14. Brinker CJ, Scherer GW (1990) Sol-gel science: the physics and chemistry of Sol-gel processing. Elsevier, pp 1–908. https://doi.org/10.1016/C2009-0-22386-5
15. Abou Hammad AB, Al-esnawy AA, Mansour AM, El Nahrawy AM (2023) Synthesis and characterization of chitosan-corn starch-SiO2/silver eco-nanocomposites: exploring optoelectronic and antibacterial potential. Int J Biol Macromol 249:126077. https://doi.org/10.1016/J.IJBIOMAC.2023.126077
16. El Nahrawy AM, Elzwawy A, Abou Hammad AB, Mansour AM (2020) Influence of NiO on structural, optical, and magnetic properties of Al2O3–P2O5–Na2O magnetic porous nanocomposites nucleated by SiO2. Solid State Sci 108:106454. https://doi.org/10.1016/j.solidstatesciences.2020.106454
17. El Nahrawy AM, Mansour AM, Abou Hammad AB (2022) Spectroscopic study of Eu3+-Doped Magnesium Lanthanum phosphate (MLPO) films on SiO2 substrate. Silicon 14:1227–1234. https://doi.org/10.1007/s12633-020-00855-x
18. El Nahrawy AM, Hemdan BA, Abou Hammad AB et al (2021) Modern template design and biological evaluation of cephradine-loaded magnesium calcium silicate nanocomposites as an inhibitor for nosocomial bacteria in biomedical applications. Silicon 13:2979–2991. https://doi.org/10.1007/s12633-020-00642-8
19. El Nahrawy AM, Abou Hammad AB, Mansour AM (2021) Preparation and characterization of transparent semiconducting silica nanocomposites doped with P2O5 and Al2O3. Silicon 13:3733–3739. https://doi.org/10.1007/s12633-021-00962-3
20. Abou Hammad AB, Mansour AM, El Nahrawy AM (2021) Ni2 + doping effect on potassium barium titanate nanoparticles: enhancement optical and dielectric properties. Phys Scr 96:125821. https://doi.org/10.1088/1402-4896/ac25a6
21. ElNahrawy AM, AbouHammad AB (2016) A facile co-gelation sol gel route to synthesize cao: P2o5: Sio2 xerogel embedded in chitosan nanocomposite for bioapplications. Int J Pharmtech Res 9:16–21
22. El Nahrawy AM, Montaser AS, Bakr AM et al (2021) Impact of ZnO on the spectroscopic, mechanical, and UPF properties of Fe2O3-tough polystyrene-based nanocomposites. J Mater Sci: Mater Electron 32:28019–28031. https://doi.org/10.1007/s10854-021-07182-w
23. El Nahrawy AM, Salah El-Deen H, Soliman AA, Mosa WMM (2019) Crystallographic and magnetic properties of Al3 + co-doped NiZnFe2O4 Nano- particles prepared by Sol-gel process. Egypt J Chem 62:525–532. https://doi.org/10.21608/ejchem.2018.4504.1397
24. Aksenov SM, Mackley SA, Deyneko DV et al (2019) Crystal chemistry of compounds with lanthanide based microporous heteropolyhedral frameworks: synthesis, crystal structures, and luminescence properties of novel potassium cerium and erbium silicates. Microporous Mesoporous Mater 284:25–35. https://doi.org/10.1016/j.micromeso.2019.04.006
25. Beainy G, Frilay C, Pareige P et al (2018) On the interplay between Si-Er-O segregation and erbium silicate (Er2Si2O7) formation in Er-doped SiOx thin films. J Alloys Compd 755:55–60. https://doi.org/10.1016/j.jallcom.2018.04.310
26. Dutchaneephet J, Limpichaipanit A, Ngamjarurojana A (2019) Optical spectroscopic investigations of neodymium and erbium added bismuth silicate glasses. Optik (Stuttg) 178:111–116. https://doi.org/10.1016/j.ijleo.2018.09.172
27. Šmejcký J, Jeřábek V, Mareš D et al (2023) Erbium–bismuth-doped germanium silicate active optic glass for broad-band optical amplification. Opt Mater (Amst) 137. https://doi.org/10.1016/j.optmat.2023.113621
28. Xue S, Bi Y, Ackah S et al (2023) Sodium silicate treatment accelerates biosynthesis and polymerization of suberin polyaliphatics monomers at wounds of muskmelon. Food Chem 417:135847. https://doi.org/10.1016/j.foodchem.2023.135847
29. Nahrawy AME, Haroun AA, Hammad ABA et al (2019) Uniformly embedded cellulose/polypyrrole-TiO2 composite in sol-gel sodium silicate nanoparticles: structural and dielectric properties. Silicon 11:1063–1070. https://doi.org/10.1007/S12633-018-9910-4
30. El Nahrawy AM, Soliman AA, Sakr EMM, El Attar HA (2018) Sodium-cobalt ferrite nanostructure study: Sol-gel synthesis, characterization, and magnetic properties. J Ovonic Res 14:193–200
31. Jamalaiah BC, Rasool SN, Rao KV et al (2023) Sensitizing effect of Yb3 + ions on 1.53 μm broadband and 548 nm upconversion green emissions of Er3+-doped TeO2–WO3–GeO2 glasses. Mater Res Bull: 112628. https://doi.org/10.1016/j.materresbull.2023.112628
32. Talewar RA, Mahamuda S, Swapna K et al (2021) Sensitization of Er3 + NIR emission using Yb3 + ions in alkaline-earth chloro borate glasses for fiber laser and optical fiber amplifier

applications. Mater Res Bull 136:111144. https://doi.org/10.1016/J.MATERRESBULL.2020.111144
33. El Nahrawy AM, Hemdan BA, Ali AI et al (2021) Sol-gel preparation of bioactive nanoporous (Al2O3: CuO: SiO2): dielectric properties and wastewater decontamination. Int J Mater Eng Innov 12:37–55. https://doi.org/10.1504/IJMATEI.2021.113216
34. Youssef AM, El-Nahrawy AM, Abou Hammad AB (2017) Sol-gel synthesis and characterizations of hybrid chitosan-PEG/calcium silicate nanocomposite modified with ZnO-NPs and (E102) for optical and antibacterial applications. Intern J Biol Macromol 97:561–567. https://doi.org/10.1016/j.ijbiomac.2017.01.059
35. El Nahrawy A, Bakr A, Abou Hammad A, Mansour A-F (2021) Nano-architecture of CaO/Ag-chitosan nanocomposite by sol gel process: formation and characterization. Egypt J Chem 64:7393–7406. https://doi.org/10.21608/ejchem.2021.80608.3995
36. Abou Hammad AB, Mansour AM, Cao F, El Nahrawy AM (2021) Effect of calcination temperature on the optical and magnetic properties of NiFe 2 O 4 - KFeO 2 nanocomposite films synthesized via WOSW Sol-gel route for opto-magnetic applications. ECS J Solid State Sci Technol 10:103016. https://doi.org/10.1149/2162-8777/ac31d2
37. Pelli S, Bettinelli M, Brenci M et al (2004) Erbium-doped silicate glasses for integrated optical amplifiers and lasers. J Non Cryst Solids 345–346:372–376. https://doi.org/10.1016/j.jnoncrysol.2004.08.046
38. Iftikhar A, Yousaf S, Ahmed Ali FA et al (2020) Erbium-substituted Ni0.4Co0.6Fe2O4 ferrite nanoparticles and their hybrids with reduced graphene oxide as magnetically separable powder photocatalyst. Ceram Int 46:1203–1210. https://doi.org/10.1016/j.ceramint.2019.08.176
39. Gaafar MS, Marzouk SY (2007) Mechanical and structural studies on sodium borosilicate glasses doped with Er2O3 using ultrasonic velocity and FTIR spectroscopy. Phys B Condens Matter 388:294–302. https://doi.org/10.1016/j.physb.2006.06.132
40. Gracie PJ, Geetha D (2023) Nano cristobalite embedded Er3 + doped multi-functional silica phosphate composite glasses for optoelectronic applications. Ceram Int 49:25848–25867. https://doi.org/10.1016/j.ceramint.2023.05.132
41. Al Helou N, Khomenkova L, Cadel E et al (2023) Optical and structural investigations of annealing impact on phase separation of Erbium-doped Al2O3 layers. Mater Sci Eng B 296. https://doi.org/10.1016/j.mseb.2023.116672
42. Saravanan S, Dubey RS (2020) Synthesis of SiO2 nanoparticles by sol-gel method and their optical and structural properties. In: Romanian Journal of Information Science and Technology. https://www.romjist.ro/abstract-641.html. Accessed 9 Feb 2024
43. Mansour AM, Hammad ABA, Nahrawy AME (2023) Study on optical of chitosan-aminopropyltriethoxysilane-SiO2 nanocomposite decorated with carbon nanotubes. Silicon 1:1–9. https://doi.org/10.1007/S12633-023-02661-7/METRICS
44. El Nahrawy AM, Montaser AS, Abou Hammad AB et al (2020) Copper lithium silicate/ZrO2 nanoparticles-coated kevlar for improving UV-Vis absorbance/ protection properties. Silicon 12:1743–1750. https://doi.org/10.1007/s12633-019-00271-w
45. Al-Hilli MF, Al-Rasoul KT (2013) Characterization of aluminosilicate glass/kaolinite composite. Ceram Int 39:5855–5862. https://doi.org/10.1016/j.ceramint.2012.12.102
46. El Nahrawy AM, Abou Hammad AB, Mansour AM (2021) Compositional effects and optical properties of P2O5 doped magnesium silicate mesoporous thin films. Arab J Sci Eng 46:5893–5906. https://doi.org/10.1007/s13369-020-05067-4
47. Mansour AM, Fathi AM, Abou Hammad AB, El Nahrawy AM (2023) Microstructures, optical and electrochemical properties of advanced Fe $_{0.8}$ Se $_{0.14}$ Si $_{0.06}$ MoO $_{4}$ nanocrystalline for energy storage applications. Phys Scr 98:055922. https://doi.org/10.1088/1402-4896/acc9ea
48. Hammad ABA, Magar HS, Mansour AM et al (2023) Construction and characterization of nano-oval BaTi0.7Fe0.3O3@NiFe2O4 nanocomposites as an effective platform for the determination of H2O2. Sci Rep 13:9048. https://doi.org/10.1038/s41598-023-36076-6
49. Abou Hammad AB, Mansour AM, Elhelali TM, El Nahrawy AM (2023) Sol-gel/gel casting nanoarchitectonics of Hybrid Fe2O3–ZnO/PS-PEG nanocomposites and their optomagnetic properties. J Inorg Organomet Polym Mater 33:544–554. https://doi.org/10.1007/s10904-022-02519-2
50. El Nahrawy AM, Ali AI, Mansour AM et al (2022) Talented Bi0.5Na0.25K0.25TiO3/oxidized cellulose films for optoelectronic and bioburden of pathogenic microbes. Carbohydr Polym 291:119656. https://doi.org/10.1016/j.carbpol.2022.119656
51. Abou Hammad AB, Elzwawy A, Mansour AM et al (2020) Detection of 3,4-diaminotoluene based on Sr0.3Pb0.7TiO3/CoFe2O4 core/shell nanocomposite: via an electrochemical approach. New J Chem 44:7941–7953. https://doi.org/10.1039/d0nj01074j
52. Mansour AM, Abou Hammad AB, El Nahrawy AM (2021) Sol–gel synthesis and physical characterization of novel MgCrO4-MgCu2O3 layered films and MgCrO4-MgCu2O3/p-Si based photodiode. Nano-Struct Nano-Objects 25:100646. https://doi.org/10.1016/j.nanoso.2020.100646
53. El Nahrawy AM, Mansour AM, Abou Hammad AB et al (2020) Optical, functional impact and antimicrobial of chitosan/phosphosilicate/Al2O3 nanosheets. J Inorg Organomet Polym Mater 30:3084–3094. https://doi.org/10.1007/s10904-020-01469-x
54. Mansour AM (2019) Fabrication and characterization of a photodiode based on 5′,5″-dibromo-o-cresolsulfophthalein (BCP). Silicon 11:1989–1996. https://doi.org/10.1007/s12633-018-0016-9
55. El Nahrawy AM, Abou Hammad AB, Mansour AM (2021) Structural investigation and optical properties of Fe, Al, Si, and Cu-ZnTiO3nanocrystals. Phys Scr 96:115801. https://doi.org/10.1088/1402-4896/ac119e
56. El Nahrawy AM, Mansour AM, Elzwawy A, et al (2022) Spectroscopic and magnetic properties of Co0.15Al0.25-xNi0.6 + xFe2O-4nanocomposites aided by silica for prohibiting pathogenic bacteria during sewage handling. Environ Nanotechnol Monit Manag 18. https://doi.org/10.1016/j.enmm.2022.100672
57. Mansour AM, Abou Hammad AB, Bakr AM, El Nahrawy AM (2022) Silica zinc titanate wide bandgap semiconductor nanocrystallites: synthesis and characterization. Silicon 14:11715–11729. https://doi.org/10.1007/s12633-022-01886-2